

Particle Simulations of Resonant Nanoantennas for Laser Driven Fusion

István Papp, Larissa Bravina, Mária Csete, Igor N. Mishustin, Dénes Molnár, Anton Motornenko, Leonid M. Satarov, Horst Stöcker, Daniel D. Strottman, András Szenes, Dávid Vass, Tamás S. Biró, László P. Csernai, Norbert Kroó



FIAS Frankfurt Institute
for Advanced Studies



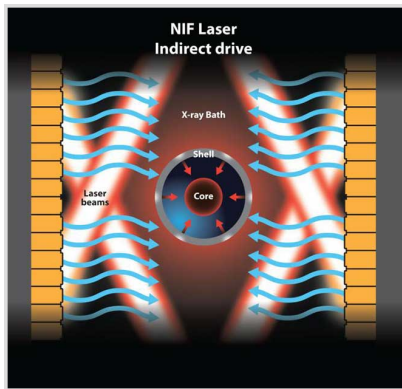
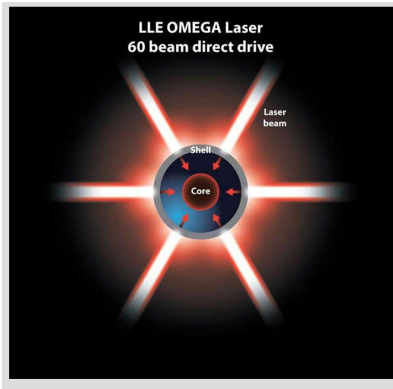
Nanoplasmonic Laser Fusion Research Laboratory



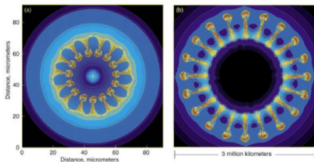
Thermonuclear Fusion

- Fusion does not happen spontaneously on Earth
- Total fusion energy $E_f = \frac{1}{4}n^2\tau\epsilon\langle v\sigma\rangle$
- ηE_f is the usable energy
- The loss is $(1 - \eta)(E_0 + E_b)$
- $E_0 = 3nkT$, $E_b = bn^2\tau\sqrt{T}$ (thermal bremsstrahlung)
- Giving the gain factor: $Q = \frac{\eta\epsilon n\tau v\sigma}{4(1-\eta)(3kT+bn\tau\sqrt{T})}$
- Q must be $Q > 1$ for energy production
- This also means $n\tau > \frac{3kT(1-\eta)}{\frac{1}{4}\epsilon\eta\langle v\sigma\rangle - b(1-\eta)\sqrt{T}} \rightarrow \text{LC}$
- Options for fulfilling the Lawson criterion
 - Magnetically confined plasmas: increase confinement time
 - Inertial confinement fusion: increase density of fusion plasma

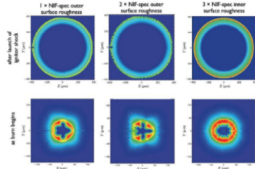
Direct vs Indirect drive



Rayleigh-Taylor instabilities



Striking similarities exist between hydrodynamic instabilities in (a) inertial confinement fusion capsule implosions and (b) core-collapse supernovae explosions. Image (a) is from Sakagami and Nishihara, *Physics of Fluids* #2, 2715 (1990); image (b) is from Hachisu et al., *Astrophysical Journal* 368, L27 (1991).



Left: same roughness of inner and outer surface as specified for the NIF target

Center: outer surface roughness is twice the NIF level

Right: DT inner surface roughness three times larger than NIF specifications

[S. Atzeni et al., *Nucl. Fusion* 54, 054008 (2014).]

25

RFD

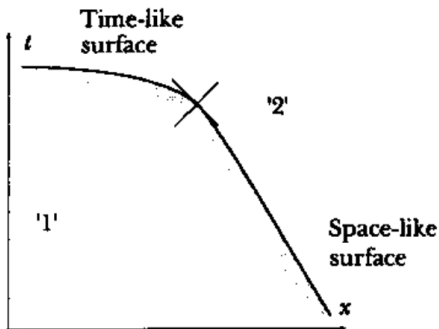
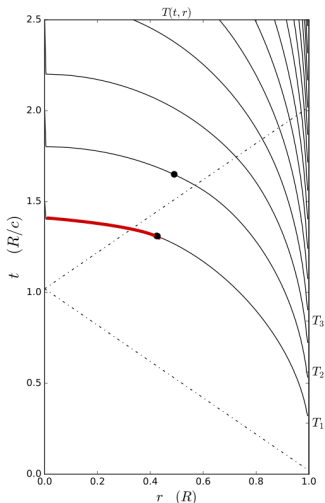


Figure 5.10: Smooth change from spacelike to timelike detonation
[Csernai, L.P. (1987). Detonation on a time-like front for relativistic systems. Zh. Eksp. Teor. Fiz. 92, 379-386.]

Constant absorptivity



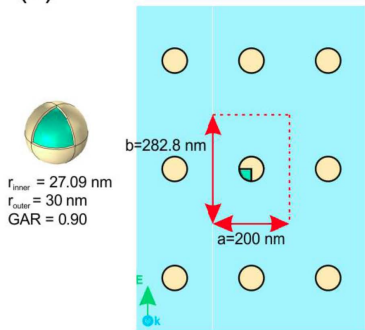
[L.P. Csernai & D.D. Strottman, Laser and Particle Beams 33, 279 (2015)]

$$\alpha_{k_{middle}} = \alpha_{k_{edge}}$$

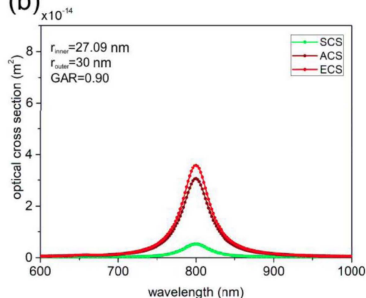
Simultaneous volume ignition is only up to 12%

Doping with gold

(a)



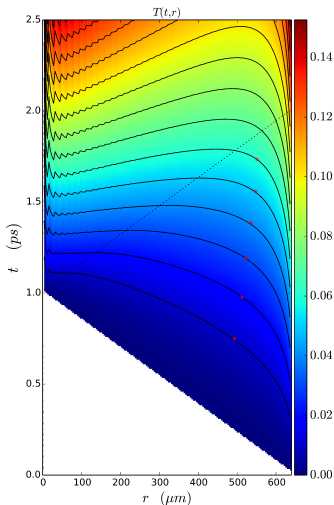
(b)



(a) Left: Single core-shell nano-sphere. Right: Rectangular lattice of nano-spheres in a transverse layer of the target.

(b) Optical cross-section of an individual core-shell nano-sphere optimized to absorb light at 800 nm wavelength and optical response of the same core-shell nano-spheres composing a rectangular lattice.

Changing absorptivity

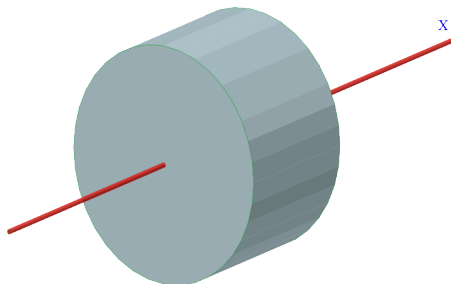


[Csernai, L.P., Kroo, N. and Papp, I. (2017). Procedure to improve the stability and efficiency of laser-fusion by nano-plasmonics method. Patent P1700278/3 of the Hungarian Intellectual Property Office.]

$$\alpha_{k_{middle}} \approx 4 \times \alpha_{k_{edge}}$$

Simultaneous volume ignition is up to 73%

Flat target

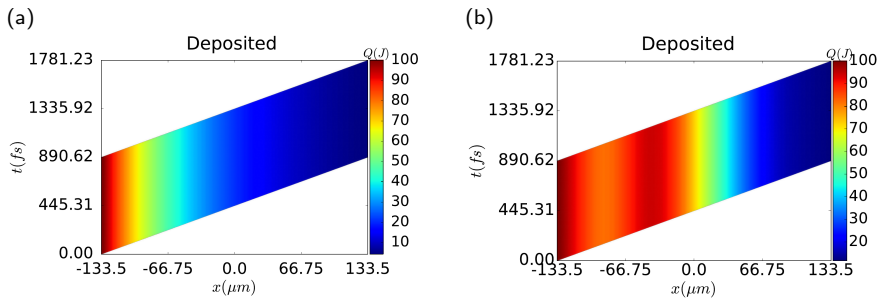


Schematic view of the cylindrical, flat target of radius, R , and thickness, h .

$$V = 2\pi R^3, \quad R = \sqrt[3]{V/(2\pi)}, \quad h = \sqrt[3]{4V/\pi}.$$

[L.P. Csernai, M. Csete, I.N. Mishustin, A. Motorenko, I. Papp, L.M. Satarov, H. Stcker & N. Kroó, Radiation- Dominated Implosion with Flat Target, *Physics and Wave Phenomena*, **28** (3) 187-199 (2020)]

Varying absorptivity



Deposited energy per unit time in the space-time plane across the depth, h , of the flat target. **(a) without nano-shells (b) with nano-shells**

To increase central absorption we used the following distribution:

$$\alpha_{ns}(s) = \alpha_{ns}^C + \alpha_{ns}(0) \cdot \exp \left[4 \times \frac{\left(\frac{s}{100}\right)^2}{\left(\frac{s}{100} - 1\right) \left(\frac{s}{100} + 1\right)} \right].$$

Particle In Cell methods

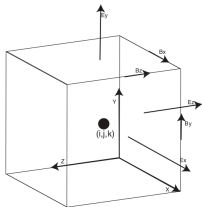


Figure 1. Yee staggered grid used for the Maxwell solver in EPOCH.

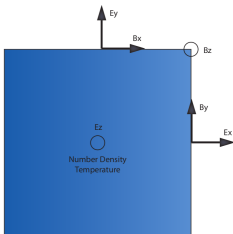


Figure 2: The Yee grid in 2D

[F.H. Harlow (1955). A Machine Calculation Method for Hydrodynamic Problems. Los Alamos Scientific Laboratory report LAMS-1956]

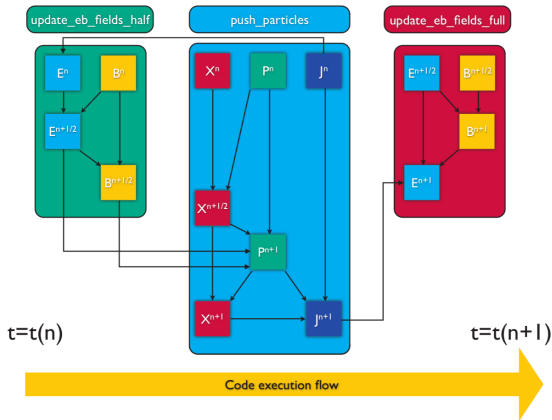
[T.D. Arber et al 2015 Plasma Phys. Control. Fusion 57 113001]

A **super-particle** (**marker-particle**) is a computational particle that represents many real particles.

Particle **mover** or **pusher** algorithm as standard **Boris algorithm**.

Finite-difference time-domain method for solving the time evolution of **Maxwell's equations**.

General layout of the EPOCH code



[EPOCH 4.0 dev manual]

- (input) deck
- housekeeping
- io
- parser
- physics_packages
- user_interaction

FDTD in EPOCH

- $\mathbf{E}_{n+\frac{1}{2}} = \mathbf{E}_n + \frac{\Delta t}{2} \left(c^2 \nabla \times \mathbf{B}_n - \frac{\mathbf{j}_n}{\epsilon_0} \right)$
- $\mathbf{B}_{n+\frac{1}{2}} = \mathbf{B}_n - \frac{\Delta t}{2} \left(\nabla \times \mathbf{E}_{n+\frac{1}{2}} \right)$
- Call particle pusher which calculates \mathbf{j}_{n+1}
- $\mathbf{B}_{n+1} = \mathbf{B}_{n+\frac{1}{2}} - \frac{\Delta t}{2} \left(\nabla \times \mathbf{E}_{n+\frac{1}{2}} \right)$
- $\mathbf{E}_{n+1} = \mathbf{E}_{n+\frac{1}{2}} + \frac{\Delta t}{2} \left(c^2 \nabla \times \mathbf{B}_{n+1} - \frac{\mathbf{j}_{n+1}}{\epsilon_0} \right)$

Particle pusher

- Solves the relativistic equation of motion under the Lorentz force for each marker-particle

$$\mathbf{p}_{n+1} = \mathbf{p}_n + q\Delta t \left[\mathbf{E}_{n+\frac{1}{2}} \left(\mathbf{x}_{n+\frac{1}{2}} \right) + \mathbf{v}_{n+\frac{1}{2}} \times \mathbf{B}_{n+\frac{1}{2}} \left(\mathbf{x}_{n+\frac{1}{2}} \right) \right]$$

\mathbf{p} is the particle momentum q is the particle's charge \mathbf{v} is the velocity.

$\mathbf{p} = \gamma m \mathbf{v}$, where m is the rest mass $\gamma = [(\mathbf{p}/mc)^2 + 1]^{1/2}$

- Villasenor and Buneman current deposition scheme [Villasenor J & Buneman O 1992 Comput. Phys. Commun. 69 306], always satisfied: $\nabla \cdot \mathbf{E} = \rho/\epsilon_0$, where ρ is the charge density.

Particle shape

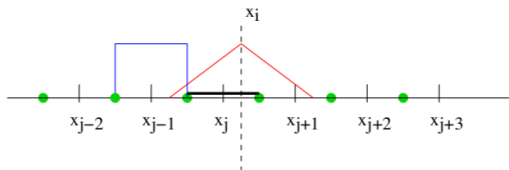


Figure 3: Second order particle shape function

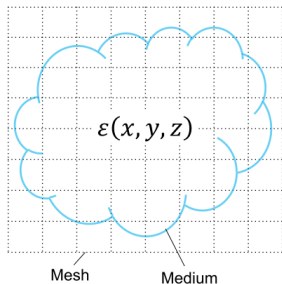
First order approximations are considered

$$F_{part} = \frac{1}{2} F_{i-1} \left(\frac{1}{2} + \frac{x_i - X}{\Delta x} \right)^2 + \frac{1}{2} F_i \left(\frac{3}{4} - \frac{(x_i - X)^2}{\Delta x^2} \right)^2 + \frac{1}{2} F_{i+1} \left(\frac{1}{2} + \frac{x_i - X}{\Delta x} \right)^2$$

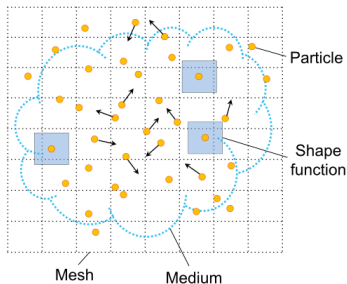
[EPOCH 4.0 dev manual]

Nanorod

A Field simulation



B Particle simulation



[W. J. Ding, et al., Particle simulation of plasmons Nanophotonics, vol. 9, no. 10, pp. 3303-3313 (2020)]

Nanorod

Field solver:

$$\epsilon(\omega) = 1 - \frac{\omega_p^2}{(\omega^2 + i\gamma\omega)}$$

where ω_p is the plasma frequency: $\sqrt{\frac{n_e e^2}{m' \epsilon_0}}$

γ is the damping factor or collision frequency: $\gamma = \frac{1}{\tau}$ and τ is the average time between collisions

Particle simulation:

$$\frac{\partial \mathbf{E}}{\partial t} = \frac{1}{\mu_0 \epsilon_0} \nabla \times \mathbf{B} - \frac{\mathbf{J}}{\epsilon_0}, \quad \frac{\partial \mathbf{B}}{\partial t} = -\nabla \times \mathbf{E}$$

$\gamma_i m_i \mathbf{v}_i = q_i (\mathbf{E}_i + \mathbf{v}_i \times \mathbf{B}_i)$, γ_i is the relativistic factor

Metal Nanoparticles as Plasmas

The conduction band electrons in metals behave as strongly coupled plasmas.

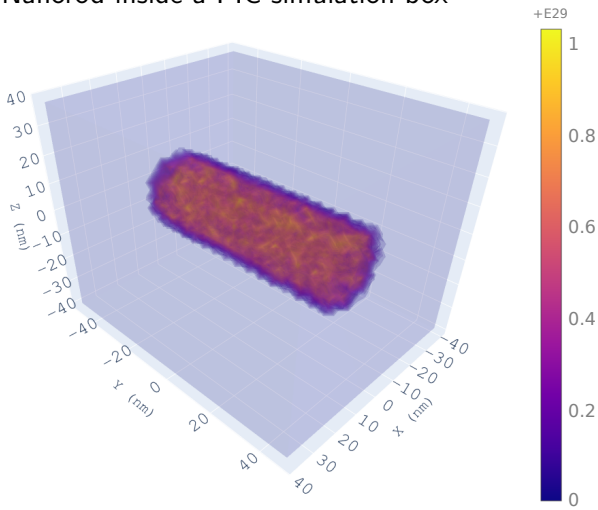
For golden nanorods of 25nm diameter in vacuum this gives an effective wavelength of $\lambda_{eff} = 266\text{nm}$

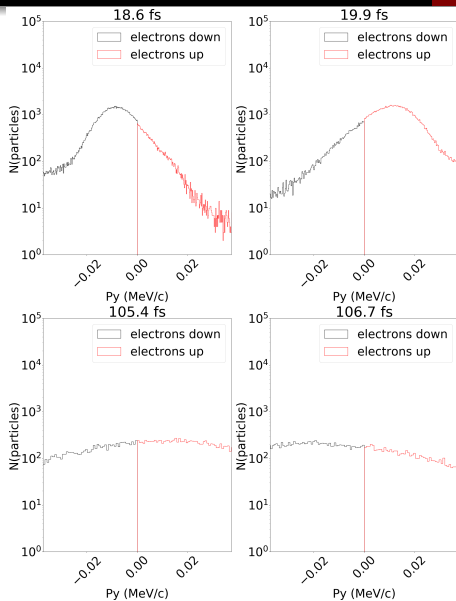
$$\frac{\lambda_{eff}}{2R\pi} = 13.74 - 0.12[\epsilon_{\infty} + 141.04] - \frac{2}{\pi} + \frac{\lambda}{\lambda_p} 0.12\sqrt{\epsilon_{\infty} + 141.04}$$

[Lukas Novotny, Effective Wavelength Scaling for Optical Antennas, Phys. Rev. Lett. **98**, 266802 (2007).]

Kinetic Modelling of the Nanorod

Nanorod inside a PIC simulation box





Considerations for the simulation box:

$$S_{CB} = 530 \times 530 \text{ nm}^2 =$$

$$2.81 \times 10^{-9} \text{ cm}^2 \text{ and length of}$$

$$L_{CB} = 795 \text{ nm}$$

beam crosses the box in

$$T = 795 \text{ nm} / c = 2.65 \text{ fs}$$

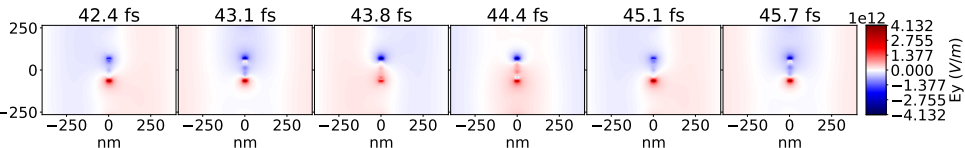
Nanorod size: 25 nm diameter
 with 75 nm length

Pulse length: $40 \times \lambda / c = 106 \text{ fs}$

Intensity: $4 \times 10^{15} \text{ W/cm}^2$

Kinetic Modelling of the Nanorod

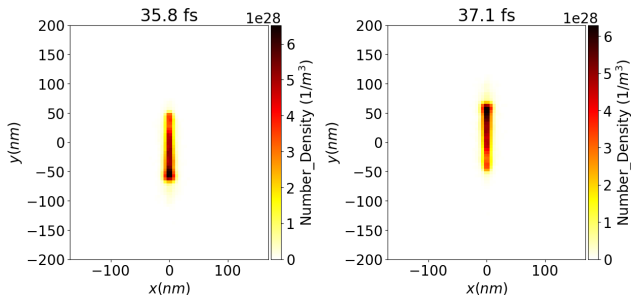
Evolution of the fields



- Evolution of the E field's y component from 42.4 till 45.7 fs, around a nanorod of 25×130 nm.
- The direction of the E field at the two ends of the nanorod does not change.

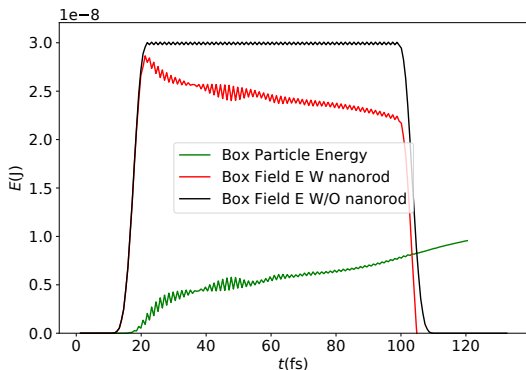
Kinetic Modelling of the Nanorod

Evolution of the nanoantenna



Number density of electrons in the middle of a nanorod of size 25x130 nm at different times. The nanorod is orthogonal to the beam direction, x .

Kinetic Modelling of the Nanorod



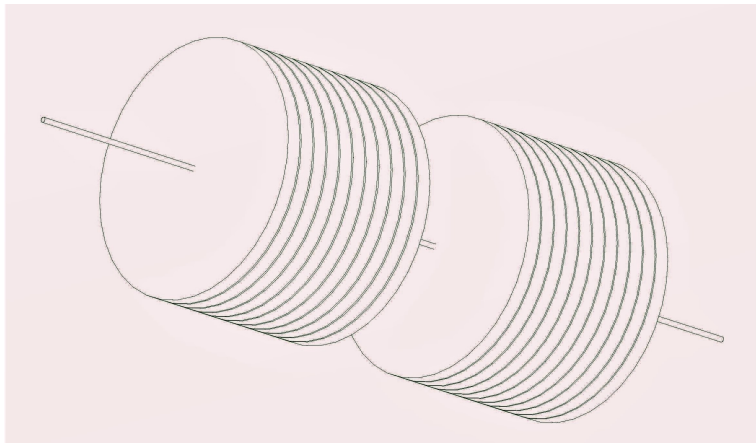
energy in the box **without nanorod** antenna 3×10^{-8} J (black line)
nanorod absorbs EM energy reducing it to 2.3×10^{-8} J (red line)
deposited energy in the nanorod (green line)

results in light absorption cross section nearly 66.5 times higher than its geometrical cross section

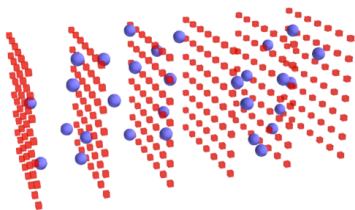
Conclusions, Looking forward

- The model returns the analytical calculations regarding the absorption cross section
- The model is highly idealized
- Next step is embedding nanorods in non-vacuum medium
- Fully dedicated software for the project is required
- Next step is estimating the target pre-compression

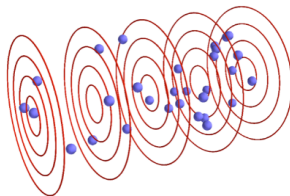
Pre-compression



Fourier-Bessel PIC method



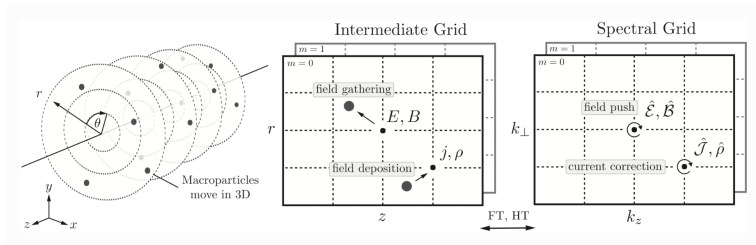
3D Cartesian grid



Cylindrical grid (schematic)

[Rémi Lehe et al., A spectral, quasi-cylindrical and dispersion-free Particle-In-Cell algorithm, *Computer Physics Communications* Volume 203]

Fourier-Bessel PIC method



[Rémi Lehe et al., A spectral, quasi-cylindrical and dispersion-free Particle-In-Cell algorithm, *Computer Physics Communications* Volume 203]

Thank you!